INTERNATIONAL JOURNAL FOR NUMERICAL METHODS IN FLUIDS
Int. J. Numer. Meth. Fluids 2006; **50**:511–530
Published online 30 September 2005 in Wiley InterScience (www.interscience.wiley.com). DOI: 10.1002/fld.1076

Three-dimensional lubrication flow of a Herschel–Bulkley fluid

Jing Zhang[1,‡], Roger E. Khayat[1,*,†] and Alphonso P. Noronha[2]

[1]*Department of Mechanical and Materials Engineering, The University of Western Ontario, London, Ont., Canada N6A 5B9*
[2]*Georg-Simon-Ohm Fachhochschule Nuernberg, Kesslerplatz 12 D-90489 Nuernberg, Germany*

SUMMARY

In this paper three-dimensional lubrication flow of grease is analysed numerically. The lubrication flow configuration is formed by two ellipsoid rollers. The load is assumed to be light enough for the lubrication mode to be purely hydrodynamic. The fluid behaviour is modelled using the Herschel–Bulkley model, and a two-dimensional modified Reynolds equation is derived. The numerical solutions are obtained by using a hybrid spectral/iterative technique and the Galerkin projection scheme. The effects of the material and geometrical parameters on pressure distribution are emphasized in the study. The investigation is conducted for a situation where the two ellipsoids are fully immersed in a grease lubricant. The effect of the geometry on the pressure distribution is determined by varying the ratio of the semi-axes and the minimum gap of the two rollers, respectively. The effect of the material parameters is examined by varying the power-law index and yield stress. It is found that the pressure distribution is strongly influenced by the shape of the rollers, the size of the minimum gap of the rollers and the rheological parameters. Copyright © 2005 John Wiley & Sons, Ltd.

KEY WORDS: non-Newtonian flow; Herschel–Bulkley model; grease lubrication; spectral method; Galerkin projection scheme

1. INTRODUCTION

The main objective of lubricants in non-conformal tribological contacts is to produce a substantially thick lubricant film between the contacting bodies, and thus prevent metal-to-metal contact. In engineering practice, non-conformal contacts can be found in a variety of machine elements such as rolling element bearings, gears, cam and cam followers. The lubricant in such contacts must be capable of producing a lubricant film under all operating

*Correspondence to: Roger E. Khayat, Department of Mechanical and Materials Engineering, The University of Western Ontario, London, Ont., Canada N6A 5B9.
†E-mail: rkhayat@eng.uwo.ca, rkhayat@uwo.ca
‡E-mail: jzhang34@uwo.ca

Received 12 April 2005
Revised 6 July 2005
Accepted 17 July 2005

conditions of the machine elements. Only the presence of a lubricant film can reduce friction and increase the operating life of tribological contacts. The practical importance of the lubricant film flow has stimulated a great deal of research, both theoretical and experimental. Significant knowledge of the pressure-build-up mechanisms and the operating lubricant film thickness in such tribological contacts for oil as a lubricant with Newtonian characteristics is well documented [1–3], while the theory of grease lubrication is far from perfect because of the complexity of its rheological properties. In practice, however, approximately 80–90% of rolling element bearings are lubricated with grease [4]. The understanding of the rheological behaviour of lubricating greases is nowadays a decisive factor in the design and optimization of the tribological systems as well as in the control of their processing. Greases are two-phase lubricants composed of a thickener dispersed in a base oil. The thickener is either a polymer fibre or a metallic soap made of a base of lithium, calcium, aluminium, sodium or synthetic. Due to the effects of the thickener, greases are often modelled as a plastic solid. Unlike oil, grease can withstand shear and will not flow until a critical yield stress is reached. Traditionally, these properties of grease have been related to the so-called 'yield state' at low strain rates and a shear-thinning behaviour at medium and high strain rates. Thus, the typical grease flow curve exhibits constant values of shear stress at low strain rates [5].

Several constitutive models have been employed in studying the grease lubrication. The two-parameter Bingham model is the one that was the earliest chosen to deal with the problem of grease lubrication. Fluids obeying this model are called Bingham plastic fluids and exhibit a linear shear stress, shear-rate behaviour after an initial shear-stress threshold has been reached. Earlier attempt at theoretical analysis of grease lubrication was reported by Sasaki *et al*. [6] who used a Bingham solid as a model for grease flowing between non-deformed cylinders. Wada *et al.* [7] used a Bingham solid as a rheological model to derive a modified Reynolds equation and obtained a numerical solution for grease film shape and pressure distribution for elastohydrodynamic lubrication. Following in these footsteps, Yang and Qian [8] derived a 2D grease lubrication equation with a Bingham model. The drawback of modelling grease lubrication with Bingham model is that the viscosity of Bingham fluids remains constant upon yielding. Experimental study conducted by Zhu and Neng [9], which dealt with the lubrication mechanism of grease in tribological contacts, showed that when grease is sheared, the apparent viscosity of the grease varies and approaches the viscosity of the base oil. Based on the available experimental data, Kauzlarich and Greenwood [10] found that most greases behave pseudo-plastically, and in the case of calcium grease, some greases will shear thicken or shear thin depending upon the shear rate.

The Herschel–Bulkley (HB) equation is one of the more realistic constitutive models for grease. HB fluids are described by a three-parameter rheological model. When the local shear stress is below the yield stress, HB fluids behave as rigid solids, similar to Bingham fluids. Once the yield stress is exceeded, unlike Bingham fluids, HB fluids flow with a non-linear stress–strain relationship either as a shear-thickening fluid, or a shear-thinning one. Grease fluids behave in this manner. Thus, the HB model is preferred to Bingham and other models because of its accurate rheological response [5, 9, 10]. Many studies on grease lubrication were conducted using the HB model. For example, Kauzlarich and Greenwood [10] derived a simplified pressure distribution equation for a grease film described by the HB model. They also validated the model experimentally. Jonkisz and Krzeminski-Freda [11, 12] obtained a numerical solution of grease lubrication problem with HB model and compared it against experiment. They also studied the effects of breakdown of the grease structure and of starvation

conditions on the film thickness. Yoo and Kim [13] first studied the thermal effect in the grease lubrication problem using HB model. They investigated the effects of temperature and rheological parameters on the minimum film thickness. Besides Bingham and HB models, a four-parameter model put forward by Bauer [14] was employed by Dong and Qian [15] to solve grease lubrication problem. Other related studies on grease lubrication can be found in References [16–19].

The previous work about grease lubrication problem was mostly focused on small film thickness formulations and pressure distribution for both hydrodynamic and elastohydrodynamic contacts. However, the full range of geometrical parameters, such as the dimensions and shape of two rollers in contact, has not been adequately studied. Brewe *et al.* [20] examined the effect of geometry on hydrodynamic film thickness for Newtonian flow. They investigated the effect of load capacity by varying the ratio of the transverse radius to the rolling radius and the dimensionless film thickness for a conjunction fully immersed in the lubricant. For the lubrication flow of HB fluids, previous studies were limited to line contact.

The current paper focuses on the grease lubrication of a fluid obeying the HB constitutive model, between two ellipsoids of arbitrary dimensions. The influence of geometrical parameters, such as the ratio of the transverse radius to the rolling radius, the dimensionless film thickness, and the HB fluid parameters, such as the power-law index, n, and the yield stress, T_0, on the pressure distribution is examined. A 3D lubrication formulation for the HB fluid is developed, and the problem is solved numerically. In particular, a fully flooded grease film between two rigid ellipsoidal solids in a pure rolling condition is examined, and a modified Reynolds equation is developed that is based on the HB model. The governing equation for pressure is developed following a procedure similar to the derivation of the conventional Reynolds equation in 3D flow under the assumption of lubrication theory.

The numerical solution of the modified Reynolds equation remains challenging despite the advent of powerfully computational techniques and platforms. Existing studies on the numerical solution of elliptic partial differential equations mostly use the Gauss–Seidel iterative method, and recently the multi-grid technique was also used [21, 22]. The multi-grid method allows a large number of nodes to be considered and significantly reduces the CPU requirement. In the present study, a combination of spectral and iterative schemes, coupled with a Newton–Raphson iteration scheme is used to solve the modified Reynolds equation.

The paper is organized as follows. The problem formulation is given in Section 2, the solution procedure is outlined in Section 3, results and discussion are given in Section 4. Finally, concluding remarks are found in Section 5.

2. PROBLEM FORMULATION

In this section, the lubrication flow configuration is introduced, and the general conservation and constitutive equations for a HB fluid, as well as the boundary conditions are briefly reviewed. The lubrication assumption is then adopted to derive the equation for the flow of a thin film.

2.1. Governing equations and boundary conditions

Consider the general steady lubrication flow of an incompressible fluid of density ρ and (Newtonian) viscosity μ, between two ellipsoids, in the (x_1, x_2, x_3) space. For simplicity, only

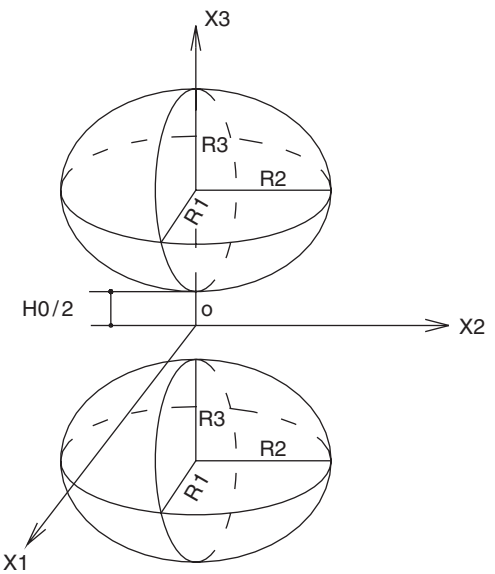

Figure 1. Schematic illustration of the lubrication flow between two ellipsoids.

symmetric flow with respect to the (x_1, x_2) plane will be considered. The extension of the formulation to more general configurations is straightforward. The situation is schematically depicted in Figure 1. The equation for the ellipsoid is

$$\frac{x_1^2}{R_1^2} + \frac{x_2^2}{R_2^2} + \frac{(x_3 - H_0/2 - R_3)^2}{R_3^2} = 1$$

where R_1, R_2 and R_3 are the semi-axes, and are assumed to be of the same order, R, and H_0 is the minimum gap between the two ellipsoids. The gap distribution is denoted by $x_3 = H(x_1, x_2)/2$. If L_1 and L_2 are two typical lengths along the lateral directions x_1 and x_2, respectively, then $L_1 \times L_2$ becomes the domain of calculation. It is, however, convenient to introduce one length scale, L, in the horizontal plane, such that $L_1 = L$ and $L_2 = \alpha L$, where $\alpha = R_2/R_1$. The dimensionless variables are defined as follows:

$$\begin{aligned} (x, y, z) &= \frac{1}{L}\left(x_1, \frac{x_2}{\alpha}, \frac{x_3}{\varepsilon}\right), \quad (u, v, w) = \frac{1}{\bar{V}}\left(u_1, \alpha u_2, \frac{u_3}{\varepsilon}\right), \quad p = \varepsilon^2 \frac{L}{\mu \bar{V}} P \\ (R, S) &= \frac{\varepsilon L}{\mu \bar{V}}(\tau_{13}, \alpha \tau_{23}), \quad (X, Y, Z, XY) = \frac{L}{\mu \bar{V}}(\tau_{11}, \alpha^2 \tau_{22}, \tau_{33}, \alpha \tau_{12}), \quad h = \frac{H}{\varepsilon L} \end{aligned} \tag{1}$$

where $\bar{V}$ is a reference velocity and $\varepsilon = L/R_1$ is the small aspect ratio. Here u_i and τ_{ij} $(i, j = 1, 2, 3)$ are the velocity vector and (symmetric) excess stress tensor components, and P is the pressure.

In this study, the fluid is assumed to obey the HB constitutive model. In this case, the excess stress tensor components are given by

$$\begin{aligned} \tau_{ij} &= \left(K\dot{\gamma}^{n-1} + \frac{\tau_0}{\dot{\gamma}}\right)\dot{\gamma}_{ij}, \quad \text{for } \tau \geqslant \tau_0 \\ \dot{\gamma} &= \quad 0, \text{ for } \tau < \tau_0 \end{aligned} \tag{2}$$

where K is a non-Newtonian 'viscosity' parameter, τ_0 is the yield stress and n is the power-law exponent. Here $\dot{\gamma}_{ij} = (\partial u_i/\partial x_j) + (\partial u_j/\partial x_i)$ are the components of the rate-of-strain tensor, and $\dot{\gamma}$ and τ are the second invariants of the rate-of-strain and excess stress tensor, respectively. They are defined by

$$\dot{\gamma} = \sqrt{\dot{\gamma}_{ij}\dot{\gamma}_{ij}/2}, \quad \tau = \sqrt{\tau_{ij}\tau_{ij}/2} \tag{3}$$

The Bingham constitutive model is recovered when $n = 1$ in Equation (2), whereas the Newtonian fluid is obtained upon setting both $n = 1$ and $\tau_0 = 0$. Finally, the power-law model corresponds to $\tau_0 = 0$ with $n \neq 1$. Similar to the Bingham fluid, Equation (2) can account for the presence of a plug flow far from the rigid boundaries.

In dimensionless form, and if terms of $O(\varepsilon^2)$ and higher are excluded, then the conservation equations of mass and momentum reduce to

$$u_x + \frac{1}{\alpha^2}v_y + w_z = 0 \tag{4}$$

$$\varepsilon^2 Re\left(uu_x + \frac{1}{\alpha^2}vu_y + wu_z\right) = -p_x + R_z \tag{5}$$

$$\varepsilon^2 Re\left(uv_x + \frac{1}{\alpha^2}vv_y + wv_z\right) = -p_y + S_z \tag{6}$$

$$p_z = 0 \tag{7}$$

where a subscript denotes partial differentiation. The Reynolds number Re (defined in terms of L) is small for most lubrication flows, and inertia effects will be neglected in this work. The effect of inertia has been extensively examined in previous studies on thin-film flow [23].

As to the boundary conditions, there is obviously a wide range of geometrical configurations and boundary kinematics that can be prescribed, with flows that can be easily accommodated by the present formulation and solution procedure. In this study, the plane (x, y) is always assumed to be a symmetry plane, which can also cover a large number of interesting flow configurations. Thus,

$$R(x, y, z = 0) = S(x, y, z = 0) = 0 \tag{8}$$

The velocity is assumed to be fully prescribed at the rigid surface, so that

$$u(x, y, z = h/2) = U(x, y), \quad v(x, y, z = h/2) = V(x, y) \tag{9}$$

where the velocity components at the boundary, U and V, will be explicitly given. Finally, since the flow is only induced by the movement of the rigid surface(s), the pressure will be taken to vanish far away.

For a HB fluid, the dimensionless shear-stress components are expressed in terms of the (dominant) shear rates, from Equation (2), as follows:

$$R = \eta u_z, \quad S = \eta v_z, \quad z \geqslant \frac{h_{\mathrm{pf}}}{2} \tag{10}$$

where a dimensionless apparent viscosity, $\eta = (T_0/\dot{\Gamma}) + \dot{\Gamma}^{n-1}$, has been introduced. Here $T_0 = \tau_0/[K(\bar{V}/\varepsilon L)^n]$ is the dimensionless yield stress, $\dot{\Gamma} = \sqrt{u_z^2 + (1/\alpha^2)v_z^2}$ is the dimensionless second invariant of the rate-of-strain tensor, and h_{pf} is the thickness of the plug-flow core. Note that the viscosity parameter has been set to $\mu = K(\bar{V}/\varepsilon L)^{n-1}$.

In the absence of inertia, Equations (5) and (6), using (7), are integrated once over the interval $[0, z]$ after substituting for the shear stresses from (10) and using conditions (8). The velocity gradients, u_z and v_z, are expressed in terms of the pressure gradients to yield, after eliminating η:

$$\dot{\Gamma} = \left[z\sqrt{p_x^2 + \frac{1}{\alpha^2}\, p_y^2} - T_0 \right]^{1/n}, \quad z \geqslant \frac{h_{\mathrm{pf}}}{2} \tag{11}$$

which, in turn, allows η to be expressed explicitly in terms of z and p. The width of the plug-flow zone is determined by setting $\dot{\Gamma} = 0$ in Equation (11):

$$h_{\mathrm{pf}} = \frac{2T_0}{\sqrt{p_x^2 + \frac{1}{\alpha^2}\, p_y^2}} \tag{12}$$

The pressure equation is obtained by integrating the continuity equation (4) over the interval $z \in [0, h/2]$, which after some algebraic manipulation gives

$$(Fp_x)_x + \frac{1}{\alpha^2}(Fp_y)_y = \frac{1}{2}(Uh)_x + \frac{1}{2\alpha^2}(Vh)_y \tag{13}$$

where

$$F(x, y) = \int_0^{(1/2)h_{\mathrm{pf}}} \int_{(1/2)h_{\mathrm{pf}}}^{(1/2)h(x,y)} \frac{z'}{\eta(x, y, z')} \mathrm{d}z' \mathrm{d}z + \int_{(1/2)h_{\mathrm{pf}}}^{(1/2)h(x,y)} \int_z^{(1/2)h(x,y)} \frac{z'}{\eta(x, y, z')} \mathrm{d}z' \mathrm{d}z \tag{14}$$

with the dimensionless gap being approximately given by

$$h(x, y) = \frac{h_0}{2} + \frac{\beta}{2}\left(x^2 + \frac{y^2}{\alpha^2} \right) \tag{15}$$

where β is the ratio of radius R_3 to R_1. The viscosity is explicitly given in terms of the pressure gradients, namely

$$\eta = T_0 \left[z\sqrt{p_x^2 + \frac{1}{\alpha^2}\, p_y^2} - T_0 \right]^{-(1/n)} + \left[z\sqrt{p_x^2 + \frac{1}{\alpha^2}\, p_y^2} - T_0 \right]^{(n-1)/n}, \quad z \geqslant \frac{h_{\mathrm{pf}}}{2} \tag{16}$$

Equation (13) is the generalized Reynolds equation for a HB fluid, and is solved subject to homogeneous conditions of the pressure at the boundary.

2.2. *Channel Poiseuille flow of a HB fluid*

To understand further the fundamental behaviour of a HB fluid, consider the channel Poiseuille flow in the (x,z) plane. A suitable velocity scale is $\bar{V} = -D^2\Delta/\mu L$, where D is the channel half-width, L is the channel length, and Δ is the imposed pressure difference. Since the flow is symmetric, only the domain $z \in [0, 1/2]$ will be considered. It is not difficult to conclude that the position of the yield surface is given by $h_{\mathrm{pf}} = 2T_0$, which is the same as that corresponding to a Bingham fluid [24]. This value is also in agreement with the more general expression (12) in the limit $p_y = 0$ and $p_x = 1$. The velocity in this case is determined as

$$u(z) = \begin{cases} n\left[\left(\frac{1}{2}-T_0\right)^{(n+1)/n} - (z-T_0)^{(n+1)/n}\right] \Big/ (n+1), & \dfrac{h_{\mathrm{pf}}}{2} = T_0 \leqslant z \leqslant \frac{1}{2} \\ n\left[\left(\frac{1}{2}-T_0\right)^{(n+1)/n}\right] \Big/ (n+1), & z < \dfrac{h_{\mathrm{pf}}}{2} = T_0 \end{cases} \tag{17}$$

The Newtonian limit is recovered upon setting $T_0 = 0$ and $n = 1$, namely $u(z) = (1-z^2)/8$. Thus, the basic Poiseuille flow (17) of a HB fluid consists of an unyielded region $|z| < h_{\mathrm{pf}}/2 = T_0$ in the channel centre, where the viscosity is effectively infinite, bounded by two yielded regions for $h_{\mathrm{pf}}/2 = T_0 \leqslant |z| \leqslant \frac{1}{2}$, in which there is a nonlinear variation in the effective viscosity. This behaviour is typically illustrated in Figure 2, where the influence of the power-law index on the velocity (Figure 2(a)) and viscosity profiles (Figure 2(b)) is shown for $T_0 = 0.1$ and the range $n \in [0.8, 1.2]$. The overall influence of T_0 and n on the flow rate, Q, is shown in Figure 2(c). In the yielded region, the velocity profile is close to parabolic for small n, and becomes close to linear for large n. The linear dependence is apparent upon taking the limit $n \to \infty$ of $u(z)$ in (17). It is interesting to observe from Figure 2(a) the unexpected essentially linear dependence of the (plug-flow) velocity on n in the unyielded core given the highly nonlinear expression in (17). In general, the overall viscosity decreases with n, and also the viscosity increases from its (minimum) value at the wall, but eventually levels off near the unyielded core. The decay becomes sharper as n increases. Indeed, in the limit $n \to \infty$, $\eta \to 1 + T_0$ and ∞ in the yielded and unyielded regions, respectively. In this case, η exhibits a discontinuity. Another quantity of interest is the volume flow rate (once a driving pressure is imposed). In dimensionless form, the volume flow rate Q is given by

$$Q = \left(\frac{2n}{n+1}\right)\left(\frac{1}{2}-T_0\right)^{(n+1)/n}\left[\frac{1}{2} - \frac{n}{2n+1}\left(\frac{1}{2}-T_0\right)\right] \tag{18}$$

Recall that expression (18) is based on the same pressure gradient. Figure 2(c) indicates that Q generally increases with n, which is expected since it is easier for the fluid to move through the channel as the effective viscosity decreases. The flow rate is smaller for larger T_0, as this corresponds to larger unyielded core. In fact, beyond $T_0 = 0.4$, there is barely any flow that moves through the channel.

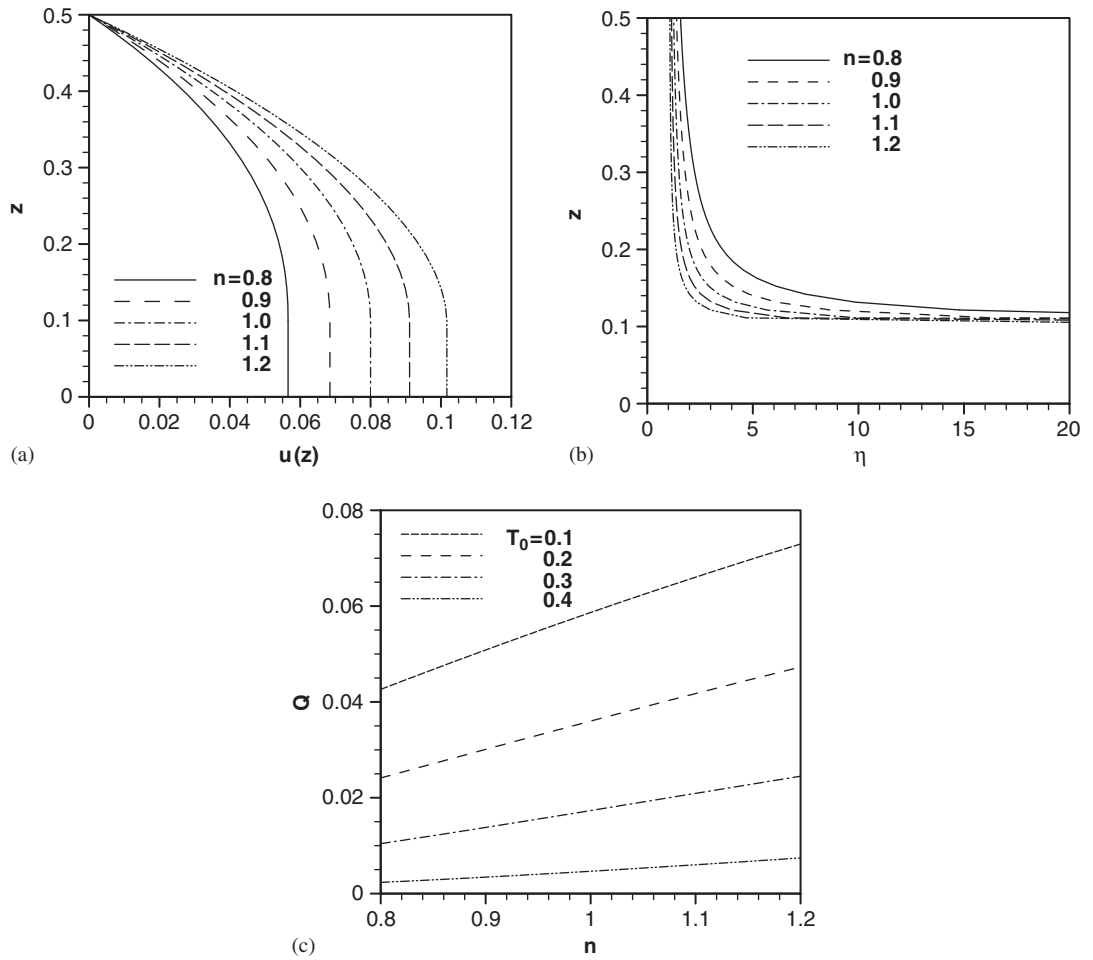

Figure 2. Symmetric channel flow of a HB fluid. Shown are: (a) the velocity profiles for $T_0 = 0.1$ and $n \in [0.8, 1.2]$; (b) corresponding effective viscosity profile; and (c) the influence of both the yield stress and power-law index on the volume flow rate. Note that the thickness of the unyielded region is independent of n.

3. SOLUTION PROCEDURE

In this section, the method of solution of Equation (13) is outlined, which consists of a hybrid spectral/iterative scheme and the Galerkin projection scheme.

3.1. Pressure expansion

The domain of computation is given by $(x, y) \in [-1/2, +1/2] \times [-1/2, +1/2]$. A general solution expansion for the pressure, which satisfies homogeneous conditions at the domain

boundary, is of the form

$$p(x,y)=\sum_{m=1}\sum_{n=1} p_{mn}\sin(2m\pi x)\cos\left[\frac{(2n-1)\pi y}{\alpha}\right] \tag{19}$$

where m and n are positive integers, and p_{mn} are unknown coefficients. Upon substitution of expression (19) into Equation (13), and using the Galerkin projection, we obtain

$$\sum_{m=1}\sum_{n=1} p_{mn}\left\{\left[(2m)^2+\left(\frac{2n-1}{\alpha}\right)^2\right]\delta_{im}\delta_{jn}-\frac{8m}{\pi\alpha}A_{ijmn}+\frac{4(2n-1)}{\pi\alpha^2}B_{ijmn}\right\}$$
$$+\frac{2}{\pi^2\alpha}(UC_{ij}+VD_{ij})=0 \tag{20}$$

where the following matrix coefficients have been introduced:

$$A_{ijmn}=\int_{-(\alpha/2)}^{\alpha/2}\int_{-(1/2)}^{1/2}\frac{F_x}{F}\cos(2m\pi x)\cos\left[\frac{(2n-1)\pi y}{\alpha}\right]\sin(2i\pi x)$$
$$\times\cos\left[\frac{(2j-1)\pi y}{\alpha}\right]\mathrm{d}x\,\mathrm{d}y \tag{21a}$$

$$B_{ijmn}=\int_{-(\alpha/2)}^{\alpha/2}\int_{-(1/2)}^{1/2}\frac{F_y}{F}\sin(2m\pi x)\sin\left[\frac{(2n-1)\pi y}{\alpha}\right]\sin(2i\pi x)$$
$$\times\cos\left[\frac{(2j-1)\pi y}{\alpha}\right]\mathrm{d}x\,\mathrm{d}y \tag{21b}$$

$$C_{ij}=\int_{-(\alpha/2)}^{\alpha/2}\int_{-(1/2)}^{1/2}\frac{h_x}{F}\sin(2i\pi x)\cos\left[\frac{(2j-1)\pi y}{\alpha}\right]\mathrm{d}x\,\mathrm{d}y \tag{21c}$$

$$D_{ij}=\int_{-(\alpha/2)}^{\alpha/2}\int_{-(1/2)}^{1/2}\frac{h_y}{F}\sin(2i\pi x)\cos\left[\frac{(2j-1)\pi y}{\alpha}\right]\mathrm{d}x\,\mathrm{d}y \tag{21d}$$

Equations (20) form a system of linear equations with matrix coefficients determined through expressions (21). The governing equation is solved using an iterative refinement algorithm (see below).

3.2. *Iterative process*

Equation (20), subject to homogeneous boundary conditions for the pressure, is solved using an iterative scheme for the evaluation of the matrix coefficients. The first step in the process consists of dividing the computational domain into rectangular finite elements. A mesh of 30 and 30 elements in the x and y directions, respectively, is reasonably sufficient. In a typical case involving a HB fluid, the pressure gradients, $p_x(x_i, y_j)$ and $p_y(x_i, y_j)$, are first calculated for a Newtonian fluid, where (x_i, y_j) are the coordinates of node (i, j). These values are then used to calculate the h_{pf} and η for the HB fluid (for prescribed T_0 and n values)

from expressions (12) and (16), respectively. Sometimes it is necessary to incorporate an intermediate step based on an n value between 1 and the prescribed value, or a T_0 value between 0 and the prescribed value. Once $h_{\mathrm{pf}}(x_i, y_j)$ and $\eta(x_i, y_j)$ are evaluated, then $F(x_i, y_j)$ is determined by carrying out the integrals in expression (14). The same process is then repeated for each node in the domain. Using Lagrange polynomials, a continuous distribution is obtained for $F(x, y)$:

$$F(x, y) = [N_{i,j} \;\; N_{i+1,j} \;\; N_{i+1,j+1} \;\; N_{i,j+1}] \;\; [F_{i,j} \;\; F_{i+1,j} \;\; F_{i+1,j+1} \;\; F_{i,j+1}]^t \tag{22}$$

where $F_{i,j} = F(x = x_i, y = y_j)$, and the nodal interpolation functions are bi-linear functions of x and y, namely

$$N_{i,j} = \left(\frac{x - x_{i+1,j}}{x_{i,j} - x_{i+1,j}}\right)\left(\frac{y - y_{i,j+1}}{y_{i,j} - y_{i,j+1}}\right)$$

The matrix coefficients are then determined from (21) using Gauss quadrature formulae, which in turn allow the calculation of the pressure coefficients from (20). The process is repeated until convergence is attained. The numerical results are stable and the number of iterations depends on the relevant global error tolerance control. Figure 3 shows the influence of number of iterations on the convergence for a fluid with parameters $T_0 = 0.2$ and $n = 1.1$, under conditions $U = 1$, $V = 0$, $h_0 = 0.1$ and $\alpha = \beta = 1$. Here the error tolerance is set at 10^{-4}. It is typically found that two to three iterations are sufficient for acceptable convergence. The assessment of the influence of grid density on the numerical result is showed in Figure 4, where the fluid parameters and the flow conditions are the same as in Figure 3. It is found that the mesh of 30×30 elements in the x and y directions is sufficient for the results to become independent of grid density.

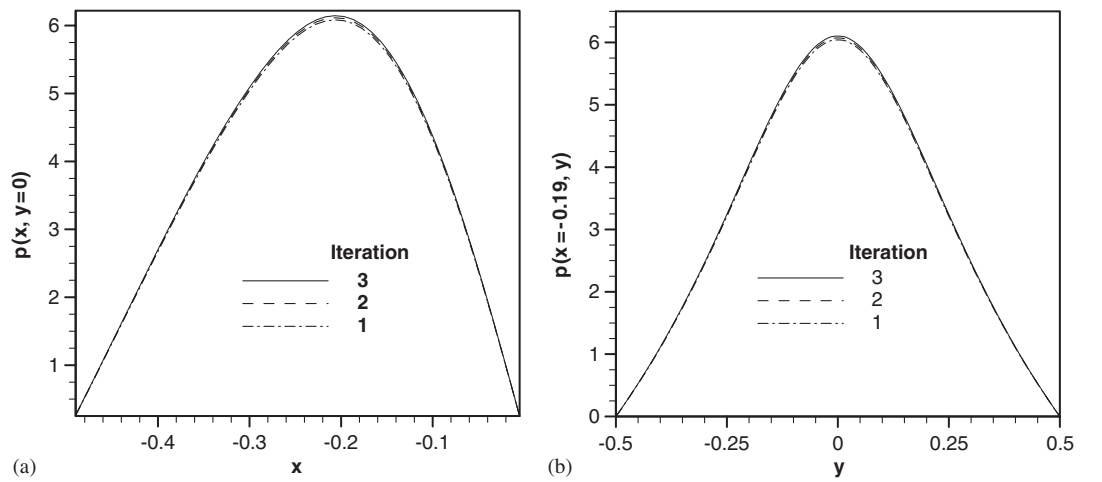

Figure 3. Influence of number of iteration on convergence. Shown are the distributions: (a) in the streamwise direction at $y = 0$; and (b) in the breadthwise direction at $x = -0.19$, for a fluid with $T_0 = 0.2$ and $n = 1.1$. Here $\beta = 1$, $h_0 = 0.1$ and $\alpha = 1$.

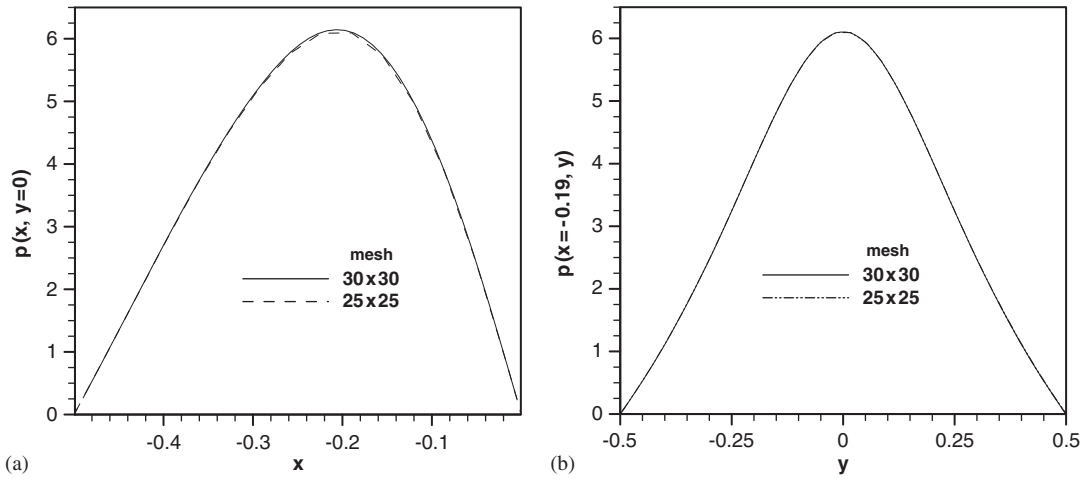

Figure 4. Influence of number of mesh on the solution dependence of grid. Shown are the distributions: (a) in the streamwise direction at $y=0$; and (b) in the breadthwise direction at $x=-0.19$. The remaining parameters are the same as in Figure 3.

4. RESULTS AND DISCUSSION

In this section, the flow of grease is examined between two ellipsoids for various flow configurations. The pressure distribution is of course crucial in lubrication flow, and it will be determined along with the flow field. The flow is examined for various ranges of geometrical as well as material parameters. The influence of geometry is examined first.

4.1. Influence of geometry

Consider first the influence of the breadth of the ellipsoid in the y direction on the flow, which is examined upon varying the value of α. This, simultaneously, will be used to assess the accuracy of the method upon comparing the results against the 2D flow between two infinite cylinders, which is reached upon setting $\alpha\to\infty$. The influence of α is depicted in Figure 5, where the pressure distribution is shown as a function of x and y for $\alpha\in[1,\infty)$, for a fluid with parameters $T_0=0.2$ and $n=1.1$. The two ellipsoids are assumed to be rolling only so that $U=1$ and $V=0$. Here $h_0=0.1$ and $\beta=1$. A 3D perspective is shown in Figure 6 for $\alpha=1$. For these parameters, $\alpha=1$ corresponds to the flow between two spheres, for which the pressure is smallest, as Figure 5 indicates. The distribution $p(x=-0.19, y)$ is essentially triangular and symmetric with respect to $y=0$, where the maximum in pressure is reached at $x=-0.19$. As α increases from 1, the overall pressure increases sharply. In particular, the pressure gradient component, p_y, increases steeply near the boundaries $y=\pm 1/2$, whereas the component p_x remains essentially unaffected by α near $x=\pm 1/2$. The case $\alpha\to\infty$ corresponds to the flow between two infinite cylinders. The pressure distribution in this case is based on the 2D flow formulation, and is taken as a limit case against which the 3D results are compared for large α. Indeed, Figure 5 shows that the 2D flow is essentially recovered for $\alpha>10$. The rate of convergence towards the 2D limit depends strongly on the fluid parameters (see next).

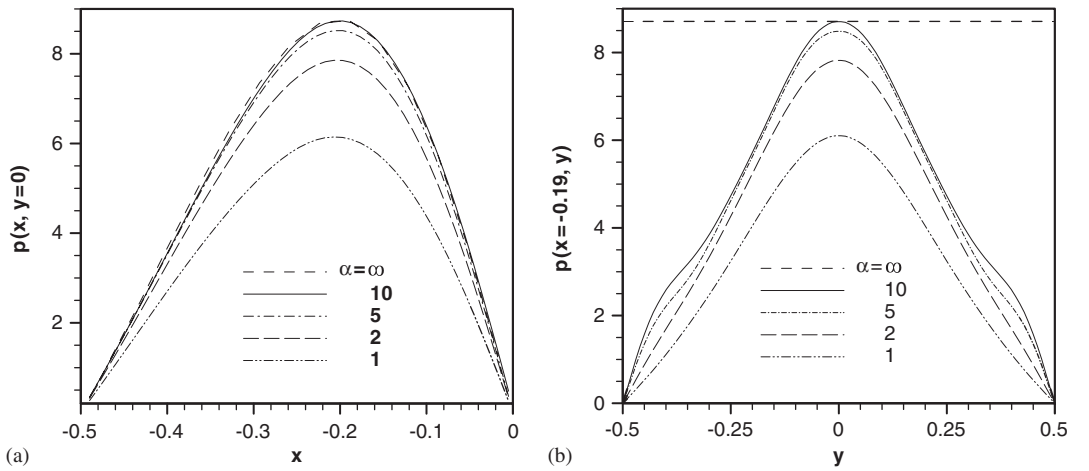

Figure 5. Influence of aspect ratio, α, on pressure distribution. Shown are the distributions: (a) in the streamwise direction at $y=0$; and (b) in the breadthwise direction at $x=-0.19$, for a fluid with $T_0=0.2$ and $n=1.1$. Here $\beta=1$, $h_0=0.1$ and $\alpha\in[1,\infty)$.

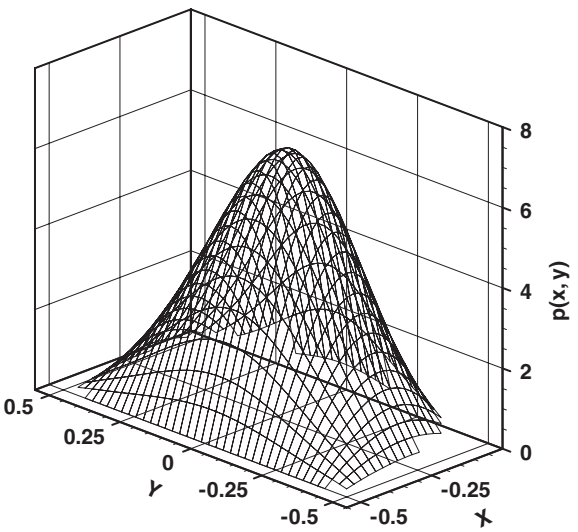

Figure 6. A 3D perspective of the pressure distribution for the flow between two spheres ($\alpha=1$). The remaining parameters are as in Figure 5.

The pressure build-up is best reflected by $p_{\max}$, the maximum value in pressure. The dependence of $p_{\max}$ on α is depicted in Figure 7, for $n=0.8$, 1.1 and 1.2, which confirms the rapid increase in pressure build-up as the shape of the ellipsoid deviates from spherical. For $n=1.1$, the pressure maximum increases with α until it begins to level off

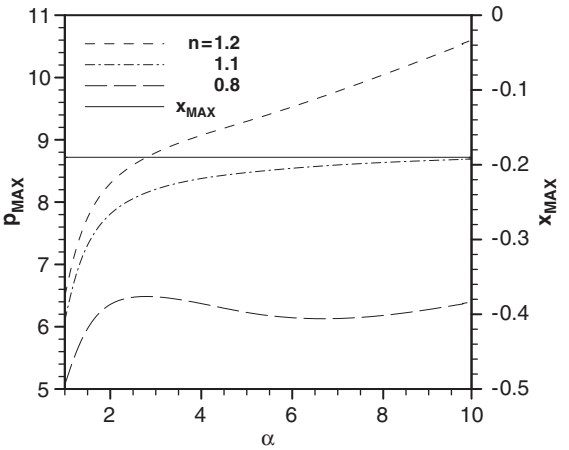

Figure 7. Dependence of maximum pressure and its streamwise location on α for the flow with parameters in Figure 3.

for $\alpha > 10$, beyond which the flow becomes essentially the same as that between two infinite cylinders. More generally, the pressure continues to increase with α (beyond $\alpha = 10$), but eventually reaches the 2D limit. The streamwise location of the pressure maximum, $x_{\max}$, is also shown in Figure 7, which appears to be independent of α. Thus, the maximum in pressure appears to occur at the same location regardless of the breadth of the ellipsoids.

Another geometrical parameter of importance is the minimum gap, h_0. Its influence is now examined over the range $h_0 \in [0.02, 0.1]$ on the flow between two spheres ($\alpha = \beta = 1$), as shown in Figure 8. The power-law index $n = 1.2$ and the remaining parameters are as before. The pressure tends to build up sharply as the gap narrows, for small gap widths ($h_0 < 0.06$). At larger gaps, the build-up is slower. This is also confirmed from Figure 9, where $p_{\max}$ and $x_{\max}$ are plotted against h_0. The maximum in pressure occurs close to the centre ($x = 0$) for small h_0, and moves upstream as the gap widens. However, a value is reached, $h_0 \approx 0.06$, beyond which the change of $x_{\max}$ is essentially inexistent.

The pressure distributions obtained in this study are similar in shape to those reported in Reference [20], which focused on geometrical effects in hydrodynamic point contacts for Newtonian flow, and concluded that the geometry (the radius ratio α) does not affect the pressure peak location but affects the magnitude of the pressure; the gap between the two rollers has remarkable influence on both the location and the magnitude of the pressure distribution. These observations are obviously in agreement with the current results.

4.2. Influence of fluid parameters

The effect of fluid parameters, namely the power-law index, n, and the yield stress, T_0, is investigated for a flow with $U = 1$, $V = 0$, $h = 0.1$, $\alpha = \beta = 1$. The influence of n on the pressure distributions, $p(x, y = 0)$ and $p(x = -0.19, y)$, are depicted in Figure 10(a) and (b), respectively, for a fluid with $n \in [0.60, 1.40]$ and a yield stress $T_0 = 0.2$. The location of

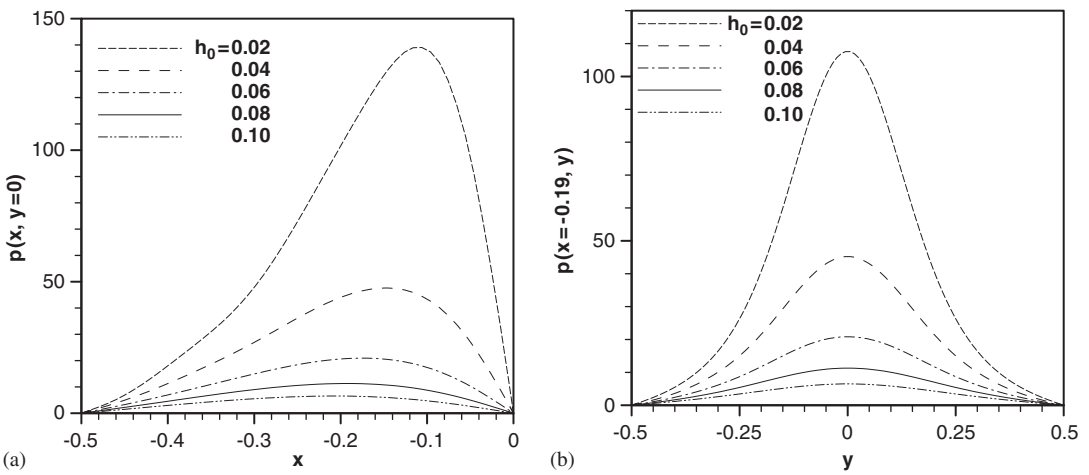

Figure 8. Influence of minimum-gap width, h_0, on pressure distribution in the: (a) streamwise; and (b) breadthwise directions, for a fluid with $T_0 = 0.2$ and $n = 1.2$. Here $\alpha = \beta = 1$.

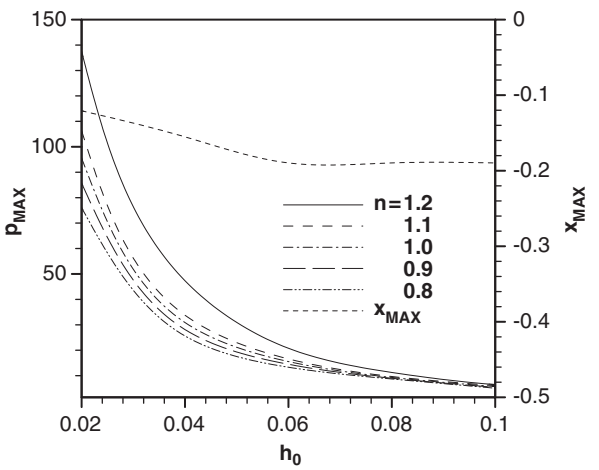

Figure 9. Dependence of maximum pressure and its streamwise location on h_0 for the flow with parameters in Figure 8.

maximum pressure is $x_{\max} \approx -0.19$, regardless of the value of n. While the power-law index has no effect on the pressure peak location, it contributes significantly to the pressure build-up. The pressure appears to increase linearly with n, at essentially every location. This result is inconsistent with the calculations of Yoo and Kim [13], who examined the (2D) non-isothermal grease elastohydrodynamic lubrication of line contacts for HB flow. The elastic deformation of the two infinitely long cylinders and the temperature effects on the grease lubrication performance were considered in their study. Johnson and Mangkoesoebroto [25]

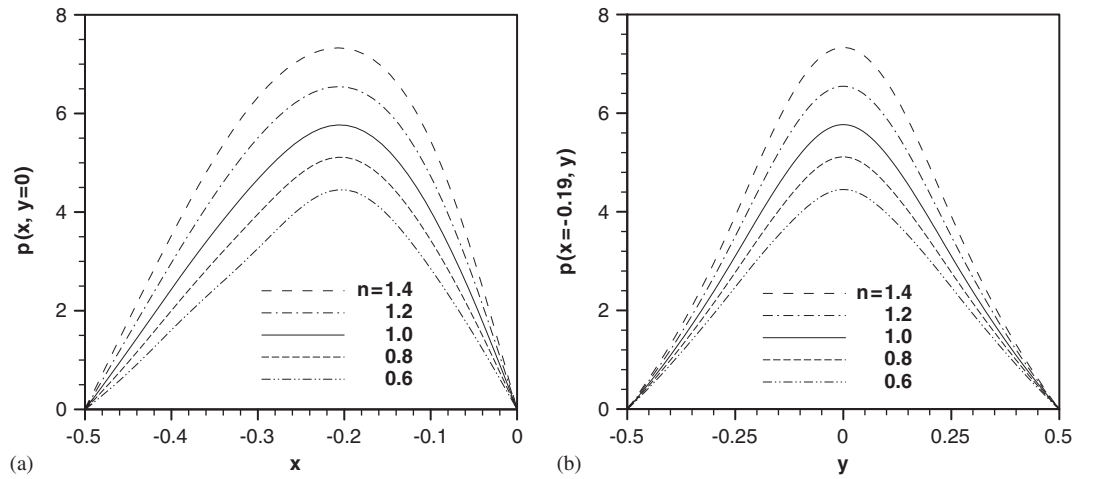

Figure 10. Influence of power-law index, n, on pressure distribution in the: (a) streamwise; and (b) breadthwise direction, for a fluid with $T_0 = 0.2$ and $h_0 = 0.1$, $U = 1$, $V = 0$. Here $\alpha = \beta = 1$.

investigated the pressure distribution of a power-law fluid between rigid walls of arbitrary shape. Their results for the influences of power-law index, n, on the pressure distribution between two spheres are consistent with the current study.

The influence of the power-law index, n, can be further assessed by examining its effect on the dimensional effective viscosity of the flow. Since the viscosity scale depends on n as it is taken equal to $\mu = K(\bar{V}/\varepsilon L)^{n-1}$, the effective viscosity is examined in its dimensional form, and is typically illustrated in Figure 11, where the viscosity is plotted against the (dimensionless) gap position in the liquid region. Figure 11 shows that the effective viscosity decreases sharply near the solid core, but levels off quickly with position. The viscosity is found to increase everywhere as n increases, which is consistent with the earlier prediction that the pressure increases with n (see Figure 10). Note that this also confirms that the pressure increases with viscosity. Figure 12 depicts the effects of T_0 on pressure for $T_0 \in [0.2, 1.0]$ and $n = 1.2$. The pressure increases with T_0, reflecting a pressure build-up as a result of the widening of the solid core. The pressure peak location is essentially unchanged (at $x_{\max} \approx -0.19$). Figure 13 shows the influence of T_0 on the effective viscosity of the flow. It shows that the larger the T_0 the higher the effective viscosity. The rate of increase of the viscosity with T_0 is, however, halted for large T_0. This behaviour is contrary to the influence of n. Figures 11 and 13 provide some guideline or means to control the value of the fluid viscosity during the flow. The overall picture is inferred from Figure 14, which shows the dependence of $p_{\max}$ on n for $T_0 \in [0.2, 0.6]$, which confirms the increase in pressure build-up for fluids with increasing greasy character. There is, simultaneously, an interesting trend observed from Figure 14. For small T_0, that is close to the Newtonian limit, the pressure maximum increases linearly with n. However, as T_0 increases, the trend becomes piecewise linear; the pressure maximum exhibits a change in slope at a critical n value that tends to decrease with T_0. This behaviour is reminiscent of phase transition phenomena in low-temperature fluids [26]. Note, finally, that the location of the pressure peak is not affected by fluid parameters.

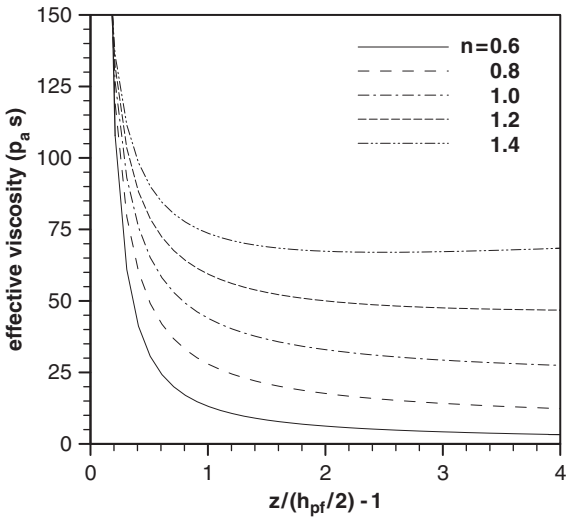

Figure 11. Influence of power-law index, n, on the effective viscosity. For a flow with $\tau_0 = 140\,\text{Pa}$, $K = 22\,\text{Pa s}^n$, $n = [0.6, 1.4]$.

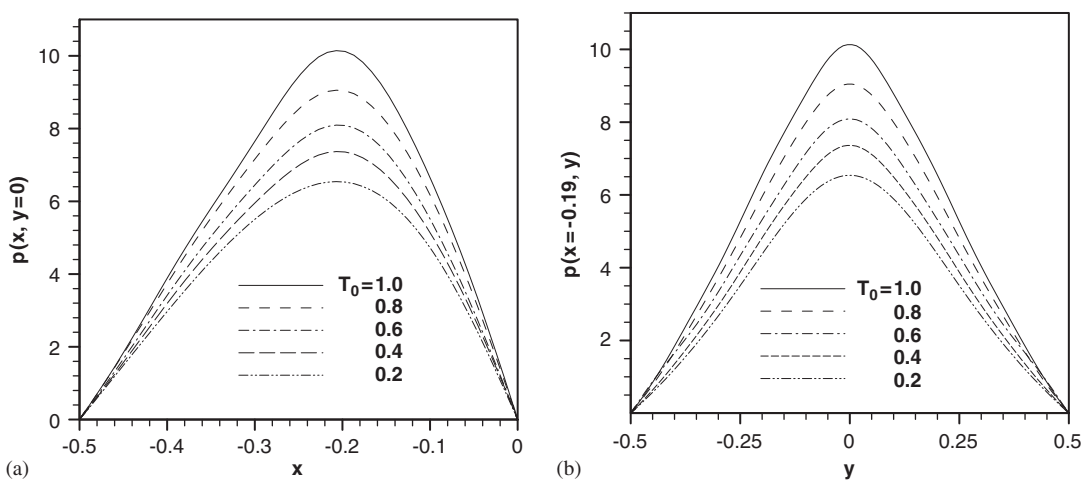

Figure 12. Influence of yield stress, T_0, on pressure distribution in the: (a) streamwise; and (b) breadthwise directions, for a fluid with $n = 1.2$ and $h_0 = 0.1$, $U = 1$, $V = 0$. Here $\alpha = \beta = 1$.

4.3. The flow field and the solid core

So far, the emphasis has been on the influence of geometrical and fluid parameters on pressure. This is, of course, understandable since the pressure build-up is of primary interest in lubrication flow. Additional insight is gained by examining the flow field and its relation to the solid core. Figure 15 depicts the velocity profiles at different locations in the plane of

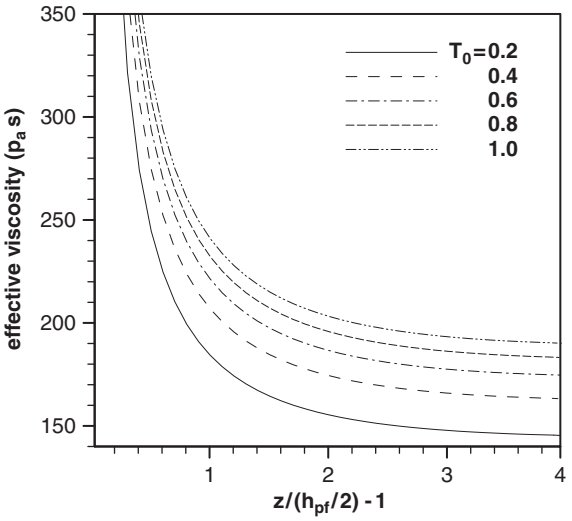

Figure 13. Influence of yield stress, T_0, on the effective viscosity. For flow with $T_0 = [0.2, 1.0]$, $n = 1.2$, $K = 22\,\mathrm{Pa\,s}^n$, $\frac{v}{\varepsilon L} = 5000\,\mathrm{s}^{-1}$.

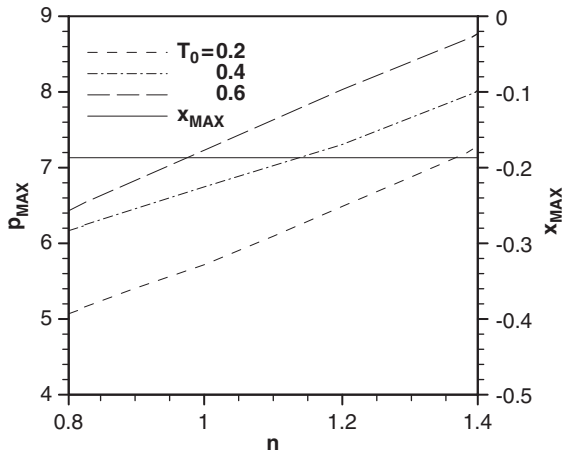

Figure 14. Dependence of maximum pressure and its streamwise location on n for the flow with the same parameters in Figure 10.

symmetry for a flow with $T_0 = 0.2$, $n = 1.2$, $U = 1$, $V = 0$, $h_0 = 0.1$, $\alpha = \beta = 1$. Figure 15(a) confirms the overall increase in u as the flow moves towards the minimum-gap region ($x = 0$). Figure 15(b) gives the distributions of the breadthwise velocity component, v. Compared with u, v is at least one-order of magnitude smaller. It is, however, not negligible as the breadthwise flow gains strength near the reservoir. The thickness of the plug-flow zone is a complex

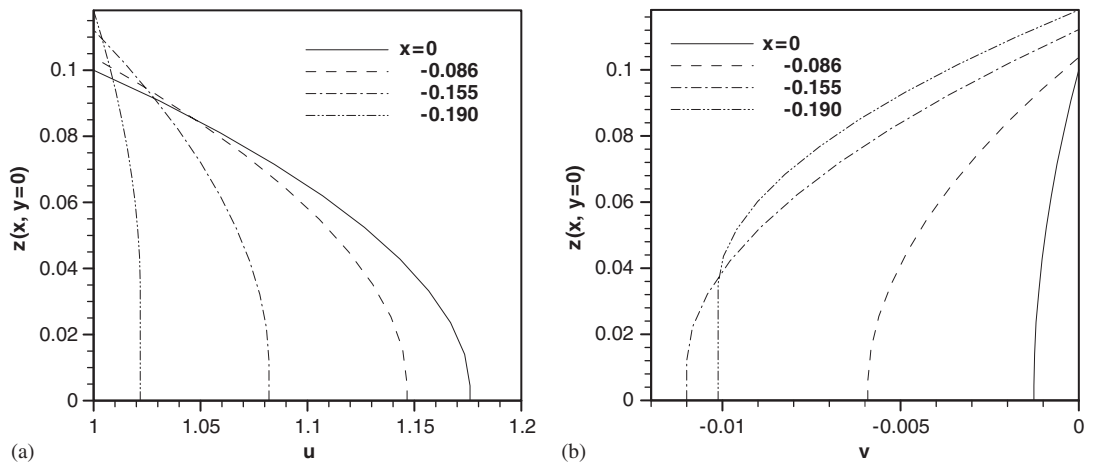

Figure 15. The velocity profile of a flow in the: (a) streamwise; and (b) breadthwise directions, with $T_0 = 0.2$, $n = 1.2$, $h_0 = 0.1$, $U = 1$, $V = 0$ and $\alpha = \beta = 1$.

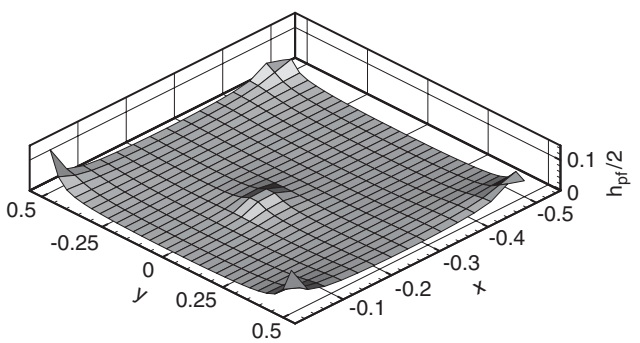

Figure 16. The plug-flow width profile with $T_0 = 0.2$, $n = 1.2$, $h_0 = 0.1$, $U = 1$, $V = 0$ and $\alpha = \beta = 1$.

function of the pressure gradient, the yield stress T_0 and the shape parameter α. It can qualitatively be inferred from the velocity distributions in Figure 15. The thickness of the plug-flow zone is typically illustrated in Figure 16. The expression for h_{pf} is recalled from Equation (12), which indicates that the plug-flow thickness is maximum at the location where the pressure gradient reaches minimum. Figure 16 indicates an enhancement of the solid core near the minimum gap and the reservoir(s), where the pressure gradient is effectively pronounced.

5. CONCLUSIONS

The 3D lubrication flow for a Herschel–Bulkley (HB) fluid is examined in this study. The study is conducted for a fully flooded grease film between two rigid ellipsoidal solids under pure rolling conditions. The numerical solution of the modified Reynolds equation is carried out using a hybrid spectral/iterative technique. The influence of the geometrical and fluid

parameters on the pressure and velocity distributions is closely examined. The effect of geometry is assessed by varying the ratio of the transverse radius to the rolling radius, α, and the minimal dimensionless gap of the two ellipsoids, h_0. The influence of fluid parameters is assessed by varying the power-law index, n, and the yield stress, T_0.

It is found that the pressure distribution exhibits a maximum, similar to Newtonian fluids. However, the peak pressure increases significantly when increasing either α, n or T_0. The peak pressure location, however, is not significantly affected by these three parameters. The minimal gap, h_0, is found to affect both the magnitude and the location of the pressure peak. As h_0 decreases, the magnitude of the pressure peak increases and the location of the pressure peak moves downstream. A critical gap ($h_0 \approx 0.06$) appears to exist, beyond which the pressure peak and location remain essentially independent of the gap. This critical value depends only very weakly on geometrical and fluid parameters.

Finally, the major contribution of the study is the treatment of 3D lubrication flow of grease, which has not been addressed before. Similar to most lubrication flow studies, the flow is not expected to be sufficiently complex for it not to be intuitively anticipatable. Obviously, much of the interesting for grease flow has already been established on the basis of 2D lubrication flow. Here the objective is to quantify further the flow behaviour as it emerges in real situations.

REFERENCES

1. Hamrock BJ. *Fundamentals of Fluid Film Lubrication*. McGraw-Hill, Inc.: New York, 1994.
2. Szeri AZ. *Fluid Film Lubrication*: *Theory and Design*. Cambridge University Press: Cambridge, 1998.
3. Dowson D, Higginson GR. *Elasto-Hydrodynamic Lubrication*. Pergamon Press Ltd.: Oxford, 1977.
4. Karbacher R. Betrieb von Waelzlagern bei hohen Drehzahlen mit rotierendem Innen-oder Aussenring. In *Einsatz von Waelzlagern bei extremen Betriebs- und Umgebungsbedingungen*, Kleinlein E (ed.), Kontakt und Studium, Band 574. Expert-Verlag, 1988.
5. Balan C, Franco JM. Influence of the geometry on the transient and steady flow of lubricating greases. *Tribology Transactions* 2001; **44**:53–58.
6. Sasaki T, Mori H, Okino N. Theory of grease lubrication of cylindrical roller bearings. *ASLE Transactions* 1960; **3**:212–219.
7. Wada S, Hayashi H, Haga K, Kawakami Y, Okjims M. Elastohydrodynamic lubrication of a Bingham solid. *Bulletin of the JSME* 1977; **20**:110–115.
8. Yang Z, Qian X. A solution to the grease lubricated EHD thickness in an elliptical contact. *Proceedings of the International Conference on Tribology*, *Institution of Mechanical Engineers 1987*, *Paper No. c347/142*.
9. Zhu WS, Neng YT. A theoretical and experimental study of EHL lubricated with grease. *Transactions of the ASME* 1988; **110**:38–42.
10. Kauzlarich JJ, Greenwood JA. Elastohydrodynamic lubrication with Herschel–Bulkley model greases. *ASLE Transactions* 1972; **15**:269–277.
11. Jonkisz W, Krzeminski-Freda H. Pressure distribution and shape of an elastohydrodynamic grease film. *Wear* 1979; **55**:81–89.
12. Jonkisz W, Krzeminski-Freda H. The properties of elastohydrodynamic grease films. *Wear* 1982; **77**:277–285.
13. Yoo J, Kim K. Numerical analysis of grease thermal elastohydrodynamic lubrication problems using the Herschel–Bulkley model. *Tribology International* 1997; **30**:401–408.
14. Bauer WH. Flow properties of soap concentration and temperature. *ASLE Transactions* 1960; **3**:215–229.
15. Dong D, Qian XL. A theory of elastohydrodynamic grease-lubricated line contact based on a refined rheological model. *Tribology International* 1988; **21**:261–267.
16. Palacios JM, Palacios MP. Theory of grease EHD contacts. *Tribology International* 1984; **17**:167–171.
17. Astrom H, Ostensen JO, Hoglund E. Lubricating grease replenishment in an elastohydrodynamic point contact. *Journal of Tribology* 1993; **115**:501–506.
18. Poon SY. An experimental study of grease in elastohydrodynamic lubrication. *Journal of Lubrication Technology* (ASME) 1972; **94F**:27–34.
19. Cheng J. Elastohydrodynamic grease lubrication theory and numerical solution in line contacts. *Tribology Transactions* 1994; **37**:711–718.

20. Brewe DE, Hamrock BJ, Taylor CM. Effect of geometry on hydrodynamic film thickness. *Journal of Lubrication Technology* 1979; **101**:231–239.
21. Kim KH, Sadeghi F. Non-Newtonian elastohydrodynamic lubrication of point contact. *Journal of Tribology* 1991; **113**:703–711.
22. Flynn EA. Grease lubrication using the Herschel–Bulkley model. *Master Thesis*, Purdue University, 1998.
23. Siddique MR, Khayat RE. Influence of inertia and topography in thin cavity low. *Physics of Fluids* 2002; **14**:1703–1719.
24. Bird RB, Armstrong RC, Hassager O. *Dynamics of Polymeric Liquids*. Fluid Mechanics, vol. 1. Wiley: New York, 1987.
25. Johnson Jr MW, Mangkoesoebroto S. Analysis of lubrication theory for the power law fluid. *Journal of Tribology* 1993; **115**:71–77.
26. Reichl LE. *A Modern Course in Statistical Physics*. The University of Texas Press: Austin, 1984.
27. Langlois WE. *Slow Viscous Flow*. The Macmillan Company, Collier-Macmillan Limited: New York, London, 1964.

